

Interfacial shear force microscopy

Khaled Karrai and Ingo Tiemann

Center for NanoScience, Sektion Physik der Ludwig-Maximilians-Universität München, D-80539 Munich, Germany

(Received 8 May 2000)

We present an experimental investigation of lossy and reactive shear forces at the nanometer scale using quartz-crystal tuning-fork shear-force microscopy. We show that this technique allows us not only to quantitatively measure viscous friction and elastic shear stress with a combination of high spatial and force resolution (better than 10 nm, and less than 1 pN, respectively), but also to obtain such quantities with the tip positioned at any arbitrary distance away from direct electrical tunnel contact with the sample surface. We are proposing that, even under vacuum conditions, the measured viscous and elastic shear stress (i.e., velocity dependent) are directly attributable to a third body filling the tip-sample gap. A simple model is given that allows us to obtain its local viscosity and shear modulus as a function of the tip-sample distance, showing that tuning-fork shear-force microscopy can be applied to quantitative analysis in nanotribology.

I. INTRODUCTION

The most fundamental property associated with friction is that the rubbing of two bodies is opposed by a resistance and accompanied by the production of heat. Not all friction interactions involve wear of material. This is particularly the case of friction due to liquids or solids that are adsorbed on the surface of atomically flat crystals. This situation is referred to as *interfacial friction*, that is, the friction that is directly attributable to atoms and molecules adjacent to the plane along which sliding occurs.¹ In recent years, significant progress was made in the investigation of interfacial friction owing to a number of new techniques that include the quartz-crystal microbalance,² the surface-force apparatus,³ and the interfacial force microscope,⁴ making it possible to study friction with geometries that are well defined at the nanometer scales.

Understanding the nature of *sliding friction* due to adsorbates is bound to have implications in the rapidly growing field of nanoelectromechanical systems (NEMS). Contamination in a form of adsorbate layers are present on almost every material exposed to normal atmospheric conditions. Due to their high surface to volume aspect ratio, NEMS are affected much more dramatically by such adsorbate contamination layers, and this in a much more dramatic way than their larger micro-electro-mechanical system counterpart.⁵ Dissipation due to adsorbed contamination is known to reduce dramatically the quality factor of nanometer-size oscillators.⁶ Even operation in a moderate vacuum do not exclude adsorbate contamination of the devices.

Microfluidics, which is also a very new branch of engineering concerned with the manufacturing and technology of liquid channels with micrometer sizes,^{7,8} can also benefit from such interfacial friction studies. There, hydrodynamic boundary conditions used for predicting fluid flow in such narrow channels can no longer rely on the standard textbook approximation according to which the molecules of the fluid are completely at rest at the liquid-solid interface.⁹ This the so-called *no-slip boundary approximation* is known to be not strictly valid.¹⁰ In particular when surface roughness is greatly reduced, as it is the case for instance in lithographi-

cally defined silicon nanostructures, slippage of fluid at the boundary is expected to play an important role. There appear to be no quantitative experimental data giving the range of applicability of the universally accepted no slippage boundary condition of liquids at solid surfaces.

Finally, shear-force scanning microscopy is a very actual field of application that would greatly benefit from understanding the origin of dissipation due to adsorbates. This new type of microscopy which was born as a by-product of near-field scanning optical microscopy^{11,12} involves a shear- and drag-force interaction between a pointed tip and a flat sample. This force is used to keep the tapered optical fiber probe of a near-field scanning optical microscope at a controlled distance from the sample surface. In this mode of operation, referred to as *shear-force scanning microscopy*, the tip is dithered in a motion parallel to the surface of a sample. It was found that in ambient conditions a dithering tip would experience damping at distances as far as 25 nm away from the sample surface. The physical origin of this interaction is still not properly understood. Nevertheless, shear force is commonly used in most, if not all, near-field scanning optical microscopes.

It is our goal with this work to contribute to the experimental investigation on interfacial friction at the nanometer scale and in particular to help elucidate the physical origin of tip-sample interaction in shear-force scanning microscopy.¹¹⁻¹³ We investigate such phenomena using a recently introduced experimental method, namely the tuning-fork shear-force microscopy (TSM).¹³ We show in this work that this technique allows us to quantitatively measure viscous friction and shear stress with an unprecedented combination of force and spatial resolution (better than piconewtons and 10 nm, respectively). TSM offers three fundamental novelties. First, it allows us to measure the friction forces (dissipative forces) with sensitivities about two to three orders of magnitudes better than common friction scanning force microscopes. Second, it allows us as well to measure the reactive forces that are associated with the combined local elastic properties of the sample, the tip, and the third-body filling the tip-sample gap. Third, it is not affected by jump to contact instabilities problems encountered in normal lever-based

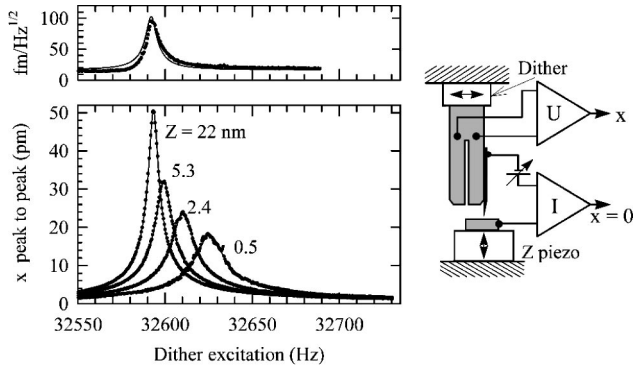


FIG. 1. Right panel: schematic experimental setup. The microscope is operated in vacuum (8×10^{-7} mbar). The tip is a cut 25- μm gold wire; the sample is atomically flat graphite or cleaved n -doped GaAs. The piezoelectric dither excites the mechanical resonance of the quartz tuning fork. The corresponding piezoelectric signal from the fork is shown in the left panel as a function of the tip-sample distance. The condition for tip-sample contact is monitored by measuring the tunnel current under a 100-mV bias. Throughout this work, the tip-sample distance $z=0$ is defined at tunnel current $I=1$ nA. The calibration of the fork signal into a tip amplitude was performed interferometrically. The gold tip is stiff and protrudes only 75 μm outside the fork's tine. The left top panel shows the noise spectrum of the tuning fork with the tip disengaged. The constant background corresponds to the Johnson noise of the amplifier, while the resonant noise corresponds to the Brownian motion of the fork tines. The measurements were performed at 300 K.

atomic force microscopes so that it is possible to position the tip in a stable way at any noncontact arbitrary distance z from the surface of a sample. This last property allows in particular to perform measurements of the z dependence of viscous friction force, a feature that was recently not possible with friction force microscopes and that was recognized by Burns *et al.*⁴

II. EXPERIMENTAL DETAILS

Quartz tuning forks were recently implemented as shear-force sensors for near-field scanning optical microscopy.¹³ We have demonstrated that their very high mechanical quality factor Q (10^3 – 10^5) provides a built-in high gain, making them very sensitive to sub-pN shear forces when used at or near their resonance frequency (10^4 – 0.5×10^6 Hz). The measurement of their mechanical oscillation amplitude uses the piezoelectric effect inherent to quartz crystals providing an electric signal proportional to the applied forces,^{13,14} rendering them small, robust, and trivial to operate compared to optical force-measurement schemes. Their sensitivity to small forces can be optimized both by increasing Q and minimizing the signal noise level down to thermodynamic limits.¹⁴ Figure 1 shows the basic geometry of a tuning-fork shear-force sensor. In order to implement tuning forks for shear-force detection it is necessary to accurately measure its fundamental mechanical resonance as a function of applied force. This can be done either by shaking the fork at its mechanical resonance and monitoring the induced voltage or by directly driving the tuning fork with a resonant voltage and measuring the induced current. On resonance, as seen in

Fig. 1, the tip is vibrating with a typical amplitude of a few tens of picometers in a motion parallel to the surface of the sample. The structure is designed to be very stiff in the direction of the sample and softer in the direction of the tip oscillation. In such a configuration, the tip is immune to the jump to contact instabilities when it is approached in the nanometer range to the sample surface.

As the probe gets closer to the sample, both dissipative and reactive forces are experienced by the tip, resulting in a decrease in the amplitude and a change in the resonant frequency of the tuning fork. This behavior is shown in Fig. 1. The probe is made out of a 25- μm -diameter gold wire sharpened into a tip, and the sample is a freshly peeled, highly oriented, pyrolytic graphite crystal. This arrangement allows simultaneous tunneling between the probe and the sample in order to indicate when the probe contacts the surface. The height z of the probe above the surface is calibrated using the onset of tunneling as the indicator of contact between the surface. We define arbitrarily $z=0$ as the condition for which the tunneling resistance is 0.1 G Ω (i.e., 1 nA under 100 mV). We were surprised to find out that even in vacuum (8×10^{-7} mbar), the tip-sample interaction was mediated at z as large as 10 nm. Assuming that a third body filling the tip-sample gap is responsible for the measured shear forces, the goal of what follows is to determine its viscosity μ and shear modulus G . In the most general case, such an interaction-mediating third body can be considered to be made out of matter (i.e., adsorbates) or fields (i.e., photons).

We found that all the measured fork's mechanical resonance spectra are very well approximated by that of a driven harmonic oscillator,¹³ indicating that there is no evidence of nonlinearity such as seen in Ref. 15 even when the tip is in tunnel interaction with the sample (at distances starting 0.5 nm). A Lorentzian fit to the resonances gives three independent sets of data, consisting of the shear oscillation maximum amplitude $x(z)$ near the tip as well as its resonance frequency $f(z)$ and its quality factor $Q(z)$. We define Q as the ratio of the resonance frequency to its width measured at full width at half maximum. Shown in Fig. 2 is an approach curve for $x(z)$ and $\Delta f(z)$, where Δf is the frequency shift of the resonance referenced to the frequency f_∞ of the unperturbed tuning fork (i.e., fully retracted tip). We do not plot the dependence $Q(z)$ since in the whole measurement range the quality factor is found to be very precisely proportional to $x(z)$, as shown in Fig. 3. These data are taken at room temperature, under vacuum conditions (i.e., 8×10^{-7} mbar) with a disengaged tip rms amplitude of $x_\infty \approx 18$ pm. The calibration of the piezoelectrical signal to the tip amplitude is obtained using differential optical interferometry.¹² A further confirmation of the small size of the tip amplitude is the fact that topographical imaging of the atomic corrugation of graphite was obtained in constant tunnel current mode while the tuning fork was excited on its resonant frequency. The onset of tunneling current measured under a 100-mV dc bias is also shown in Fig. 2. We verified that the resonance spectra did not depend in a measurable way on the applied tunnel bias voltage and this in a range between 0 and 10 V. The presented data were obtained using a commercial quartz tuning fork with tines having a static spring constant of $K=40.5$ kN/m as determined independently from Brownian noise measurements¹⁴ and the theoretically expected

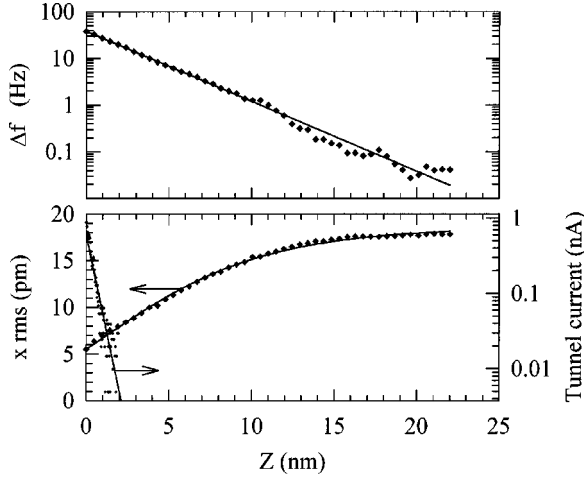


FIG. 2. The lower panel shows the maximum amplitude of the fork mechanical resonance (dots) as a function of the tip-sample distance z . The solid line is the result of the fit to Eq. (2) discussed in the text. The best fit was obtained for $x_\infty = 18.6$ pm, $\delta = 5.63$ nm, and $\lambda = 4.63$ nm. The corresponding frequency shift of the resonance position is shown in the upper panel (dots). The solid line is the result of an exponential decay function fit given by $\Delta f_0 \exp(-z/\delta_f)$, where $\Delta f_0 = 37.79$ Hz and $\delta_f = 2.90$ nm.

$K = (E/4)W(T/L)^3$, where $L = 4$ mm, $T = 0.65$ mm, and $W = 0.5$ mm, being the length, thickness, and width, respectively, of the tines. We have used the Young modulus $E = 7.87 \times 10^{10}$ N/m² of quartz. We excited the fork's resonance by mechanically dithering its center of mass with an amplitude of $x_D = 0.218$ pm rms. The piezoelectric signal is, however, proportional to the resonant mode of the relative motion of the arms. The coupling to this relative motion resonance mode is only possible through minute mass and spring constant asymmetries between the fork's tines. The gold wire probe, which was glued along the side of one of the tines as shown in the inset of Fig. 1, provides automatically such an asymmetry. The probe was electrically con-

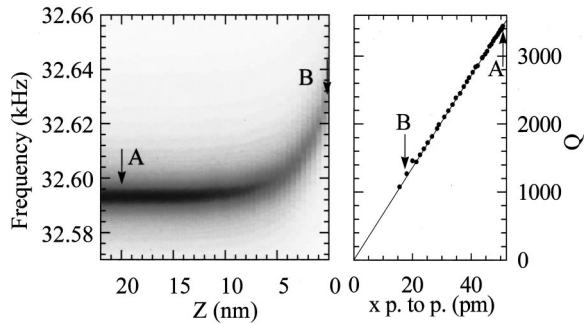


FIG. 3. Right panel: Quality factor Q of the mechanical resonance of the quartz tuning fork as a function of the tip amplitude x . Q and x reduce proportionally when the tip is approached toward the sample. This strict proportionality confirms that the friction force introduced by the tip-sample interaction is viscous (i.e., proportional to velocity). The slope is $x/Q = F_D/(K\sqrt{3})$, where F_D is the driving force and $K = 40.5$ kN/m the static spring constant of the tines. Left panel: gray-scale plot showing the measured frequency spectra as a function of the tip-sample distance. Dark areas correspond to high piezoelectric signals on the fork pads. Both marker points A and B correspond to those in the right panel.

tacted in order to monitor the tunnel current. Special care was taken so that the tip protruded only $70 \mu\text{m}$ out of the fork's tine. In this way we are confident that the tip picks up both elastic and viscous shear without appreciable bending in comparison to the tine oscillation amplitude x . The data were taken in open loop (no feedback), parking the tip at fixed distances z above the sample surface and probing the response of the fork.

III. FRICTION AND ELASTIC FORCES

We used the three sets of data $\{x, Q, f\}$ in the effective-mass harmonic oscillator approximation for the driven tuning fork in order to obtain information concerning the tip-sample interaction. In this approximation, the frequency-dependent oscillation amplitude u of the fork's arm at its ends obeys the Newton equation of motion given by $M\ddot{u} + M(\gamma + \gamma_\infty)\dot{u} + (K+k)u = F_D$. The effective mass M of the fork's arm, which is proportional to the mass distributed along the tine, is defined as $M = (K+k)/(2\pi f)^2 = 0.966 \times 10^{-6}$ kg and is about $\frac{1}{4}$ of the tine's mass.¹³ The force F_D drives the fork harmonically at a cyclic frequency ω , and the damping of the motion is included in the damping rate term $\gamma + \gamma_\infty$. The tip-sample interaction, in which we are primarily interested, introduces both an excess restoring as well as a viscous force included in the equation above through the terms k and γ , respectively. The damping rate intrinsic to the fork with the tip disengaged from the sample is γ_∞ . On resonance condition, for which $\omega = 2\pi f$ and $u = x$, it is easy to show that $\gamma + \gamma_\infty = (F_D/M)(1/\omega x)$. We can then determine the tip-sample-interaction-induced damping rate in relation to γ_∞ , which is given by $\gamma = \gamma_\infty [f_\infty x_\infty / (fx) - 1] \approx \gamma_\infty [x_\infty / x - 1]$, where the subscript ∞ refers to corresponding resonance parameters of the fully disengaged tip (i.e., z at infinity). The fork internal damping rate is also given by $\gamma_\infty = 2\pi f_\infty / (\sqrt{3}Q_\infty)$. The product $M\gamma$ is a rate of a mass colliding with the tip, which is information that can be used in order to select among possible mechanisms accounting for the tip-sample viscous interaction. The damping rate obtained using the formula above is plotted in Fig. 4. Similarly, the local tip-sample-interaction equivalent spring constant k can be obtained in relation to K . It is obtained using both resonance equations $(2\pi f)^2 = (K+k)/M$ and $(2\pi f_\infty)^2 = K/M$. The local spring constant k is then given by $k = [(f/f_\infty)^2 - 1]K$, which is plotted in Fig. 4. It is interesting to note that both γ and k are very well approximated by an exponential decay behavior. The best fit to the data is given by $\gamma = \gamma_0 \exp(-z/\delta_\gamma)$, where $\gamma_0 = 72.0 \text{ s}^{-1}$, $\delta_\gamma = 4.02$ nm, and $k = k_0 \exp(-z/\delta_k)$, where $k_0 = 93.9$ N/m and $\delta_k = 2.90$ nm. Such a behavior would be, in principle, expected in the tunneling regime. Our measurements indicate, however, that the tip is most of the time out of tunneling and this cannot be the explanation for such a behavior. The friction force $F_V = M\gamma\dot{x}$, which is due to the tip-sample viscous damping, is a drag force opposing the oscillatory motion of the tip. Using the equations for γ , γ_∞ , and M we determine

$$F_V = \frac{i}{\sqrt{3}} \left(1 - \frac{fx}{f_\infty x_\infty} \right) \frac{Kx_\infty}{Q_\infty}, \quad (1a)$$

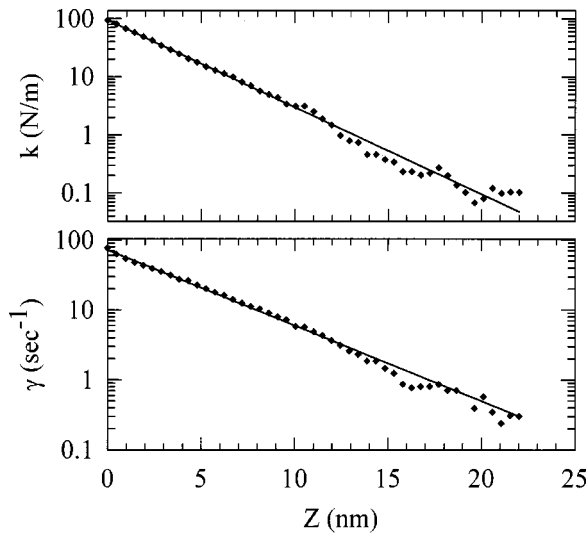


FIG. 4. The lower panel shows γ , the damping rate contribution of the tip-sample interaction. The quantity $M\gamma$ corresponds to a mass rate of colliding events picked up by the tuning fork. M is the effective mass of the tine. The upper panel shows the effective spring constant introduced by the tip-sample interaction. While γ is purely a lossy term in the harmonic oscillator, k is a reactive term. Both terms are well approximated by exponential decay (solid lines) function given by $\gamma = \gamma_0 \exp(-z/\delta_\gamma)$, where $\gamma_0 = 72.0 \text{ s}^{-1}$, $\delta_\gamma = 4.02 \text{ nm}$, and $k = k_0 \exp(-z/\delta_k)$ where $k_0 = 93.9 \text{ N/m}$, $\delta_k = 2.90 \text{ nm}$.

where the imaginary term i indicates that the friction is $\pi/2$ out of phase with the tip motion and the square root of 3 originates from the definition of Q given above. The elastic force F_E due to the reactive tip-sample interaction, which is a restoring force along the oscillation motion of the tip, can be also trivially obtained by calculating $F_E = kx$:

$$F_E = \left(\frac{f^2}{f_\infty^2} - 1 \right) Kx. \quad (1b)$$

Both forces are plotted as a function of the tip-sample distance in Fig. 5, where it can be seen that the tuning-fork shear-force sensor allows for detection with a few piconewton resolution. The force resolution is limited by noise in x_∞ , which in our present case is $0.1 \text{ pm/Hz}^{1/2}$ and is the thermodynamic limit given by the quadrature sum of the Brownian motion of the tines and the Johnson noise of the load resistor of the signal amplifier. These limits were carefully analyzed and documented in a previous publication.¹⁴ Decreasing the temperature would allow us to operate with a smaller free oscillating amplitude x_∞ . Equations (1a) and (1b) show that further improvement to friction sensitivity can be achieved by increasing the fork's quality factor Q_∞ and decreasing its arm spring constant K .

We now address an important question concerning the validity of the viscously damped driven harmonic oscillator model for the measured tip-sample interaction. In such a model the viscous forces are assumed to be proportional to velocity. The consequence of this is that Q must be proportional to x . The relation between Q and x is plotted in Fig. 3, and it is found to follow very accurately a proportionality dependence. This is different from direct solid-solid contact

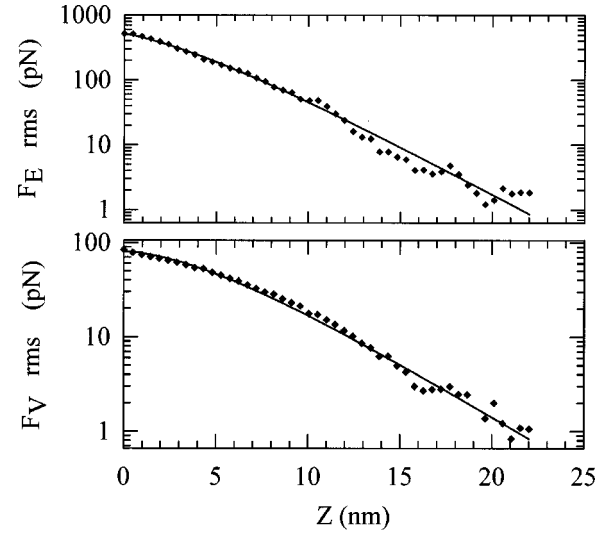


FIG. 5. The lower panel shows the viscous (friction) force experienced by the tip, and the corresponding restoring elastic force is shown in the upper panel. The data (dots) are obtained using the data set $\{x, f\}$ and Eqs. (1a) and (1b). The solid lines are the result of the fitted functions for x , k , and, γ used in conjunction with Eqs. (1a) and (1b). To the best of our knowledge, the friction forces shown here are the smallest reported in scanning probe microscopy.

friction, which is not a function of the velocity but rather is proportional normal loading force. Clearly the friction we are measuring here is not dominated by slip-stick mechanisms as in solid-solid contact friction. The tip oscillation amplitude is always smaller than typical interatomic spacing; hence the slip-stick type of friction is not possible here. From the slope $Q(x)$ we can deduce the amplitude of the force driving the harmonic oscillator. It is easy to show that the force driving the relative motion mode of the tines is $F_D = \sqrt{3}Kx(z)/Q(z)$, which we evaluate to here be 116 pN rms . This contrasts with the driving force of the center of mass of the tines, which is $M\ddot{x}_D = Kx_D = 8.8 \text{ nN}$, where x_D is the dither amplitude given above. The coupling efficiency of the mechanical dithering of the center of mass to the relative motion mode is therefore of only 1.3%. A much more efficient coupling can be obtained by exciting electrically the fork.¹⁴ In spite of such a poor coupling it is important to note that the dither amplitude remains small compared to the tip amplitude $x(z)$ and this is true for all distances z .

A first inspection of the tip-sample interaction results plotted in Figs. 4 and 5 shows that the tip experiences a shear- and friction-force interaction at distances as large as 15 nm away from the sample surface. This is unexpected, considering that the measurement took place in a high-vacuum environment. Another important point to note is that the tip peak-to-peak oscillation amplitude was always less than 0.05 nm . Consequently, here the subatomic amplitude of the tip motion precludes mechanical tapping with the sample surface. This is in contrast with many shear-force instruments running at $\sim 1\text{--}10 \text{ nm}$ (Refs. 11 and 12) amplitude, a different regime that may include some tapping.¹⁵ Also we would like to point out that all data shown in this work were taken while the tip approached the sample. When the tip comes into a tunnel interaction with the graphite surface, the retracting curve does not retrace the approach

curve. This hysteretic behavior is found most pronounced on graphite samples, but often weak or nonexistent on cleaved GaAs semiconductor (n -doped) samples. We attribute for now the existence of this hysteresis to the fact that the graphite is a system of stacked weakly bound layers. As a consequence it is much more compliant along the surface normal than the GaAs.

IV. VISCOSITY AND SHEAR MODULUS

We would like now to evaluate the coefficient of viscosity μ as well as G , the shear modulus of the hypothetical third body filling the tip-sample gap. The shear stress acting along x in the plane z in this third body is given by $\sigma_{V,xz} = \mu \partial \dot{x} / \partial z$ and $\sigma_{E,xz} = G \partial x / \partial z$, where the viscous stress $\sigma_{V,xz}$ is the product of the viscosity with the shear rate and $\sigma_{E,xz}$ is the elastic stress. The corresponding shear forces are simply $F_V = A \sigma_{V,xz}$ and $F_E = A \sigma_{E,xz}$, where A is the effective area of interaction between tip and sample. Equating these two relations with the expressions of the forces determined above leads to two time-independent differential equations $M \gamma \dot{x} = A \mu \partial \dot{x} / \partial z$ and $kx = AG \partial x / \partial z$ from which we deduce the equality $\mu / (M \gamma) = G / k$. Since we have observed in Fig. 4 that γ and k are well approximated with two exponential functions with different decay lengths, the above condition imposes that μ and G must also have a decaying exponential behavior of the type $\mu = \mu_0 \exp(-z/\delta_\mu)$ and $G = G_0 \exp(-z/\delta_G)$, where μ_0 and G_0 could also depend on z provided that they have the identical functional dependence. The two new decay lengths must obey $1/\delta_\gamma - 1/\delta_\mu = 1/\delta_k - 1/\delta_G$. We will assume for now that both $A \mu_0$ and $A G_0$ are constant with respect to z and we will check later that this hypothesis is consistent with the prediction for $x(z)$. Solving both differential equations for $x(z)$ we obtain the functional form

$$x(z) = x_\infty \exp\left[-\frac{\delta}{\lambda} \exp\left(-\frac{z}{\delta}\right)\right] \quad (2)$$

for which the following conditions must be satisfied: $1/\delta_\mu = 1/\delta_\gamma - 1/\delta$ and $1/\delta_G = 1/\delta_k - 1/\delta$ as well as $\mu_0 = \lambda(M \gamma_0 / A)$ and $G_0 = \lambda(k_0 / A)$. We have fitted the measured x with the functional form above. The best fit was obtained for $x_\infty = 18.6$ pm, $\delta = 5.63$ nm, and $\lambda = 4.63$ nm and is plotted in Fig. 2. The quality of the fit is convincing enough to tell that the assumption made above is reasonable. In fact we expect that the contact area A should be a function of z . In all our experiments however, A is not known with satisfactory accuracy in order to obtain a precise quantitative value of G and μ . For the presented measurements, we estimate A to be bracketed in the range $(30 \text{ nm})^2$ to $(100 \text{ nm})^2$ and is expected to scale linearly with the tip radius as we will show it below. Such contact areas would correspond to a tip radius bracketed between 30 and 100 nm, which is always larger than the tip-sample distances measured here making the assumption of constant A reasonable. Equation (2) shows that the maximum damping of the resonance amplitude for $z=0$ given by $x(0)/x_\infty = \exp(-\delta/\lambda)$ is not necessarily 0. We discuss now the meaning of the lengths δ and λ . Remembering that $\gamma_0 \approx \gamma_\infty [x_\infty/x(0) - 1]$, we obtain $\delta/\lambda \approx \ln(\gamma_0/\gamma_\infty + 1)$ which shows as expected that stronger damping [i.e.,

$x(0)/x_\infty$ small] is obtained with sensitive forks (i.e., γ_∞ small). Knowing the expression of λ from the conditions related to Eq. (2) above we deduce that the length $\delta \approx [\mu_0 A / M \gamma_0] \ln(\gamma_0/\gamma_\infty + 1)$ reflects a characteristic interaction distance between the tip and the sample, which also includes the sensitivity of the shear-force sensors in the fork damping rate γ_∞ . An inspection of Eq. (2) shows that the shear-force sensors is expected to be more sensitive to a third-body filling for larger values of δ . In particular, tuning-fork sensors with poor Q_∞ (i.e., γ_∞ large) leads to short δ ; hence the detection of the tip-amplitude damping is poor. In particular, when the term γ_0/γ_∞ in the logarithm above is small compared to unity, the length δ is also proportionally small. The term $\lambda = \mu_0 A / M \gamma_0$ in front of the logarithm in the expression of δ appears to depend on the tip size as well as the fork-tine mass. We will show now that in fact it depends solely on the fundamental properties of the third body. The viscosity is $\mu_0 = \rho \eta$, where ρ is the density and η the specific viscosity (in units of m^2/s) of the unknown third body. The quantity $M \gamma_0$ is the effective colliding mass rate detected by the fork sensor, which can be expressed as $M \gamma_0 = \rho V_{\text{eff}} / \tau$, where τ is a scattering time related to the viscosity and V_{eff} the effective volume of contributing scattering particles in the third body. This can be rewritten as $M \gamma_0 = \rho A z_0 / \tau$, where z_0 is an effective length specific to the third body. Consequently the term $\lambda = \mu_0 A / M \gamma_0 = \eta \tau / z_0$ is a constant of the third body and does not depend on the tip geometry and sensor specifications, implying that γ_0 is proportional to $\mu_0 A / M$. We verified the expected behavior of λ and δ experimentally by measuring approach curves obtained for several tip-sample contact areas. The approach curve measurements and their corresponding fit to Eq. (2) are shown in Fig. 6. We find indeed that $\lambda = 5 \pm 0.5$ nm is almost constant while δ ranges from 3 to 27 nm when the contact area is significantly increased by increasing the tip radius. Unfortunately, we are not able to measure the contact area A independently. The trend shows also that a larger tip-sample interaction area results in a stronger damping upon tunnel contact conditions. Equation (2) corresponds also to the distribution of shear motion in the material filling the gap as well as the that of flow velocities. Such a functional form for the velocity distribution is potentially relevant to hydrodynamic applications in areas of microfluidics. It shows in particular that the velocity of the fluid at $z=0$ is not zero, and that the *no-slippage* approximation fails when the sample surface is atomically flat.

From the fit parameter x_∞ and δ obtained above we can generate a plot of the viscosity $\mu(z)$ and the shear modulus $G(z)$ using

$$\mu = \frac{\delta}{A \ln(x_\infty/x)} M \gamma, \quad (3a)$$

$$G = \frac{\delta}{A \ln(x_\infty/x)} k. \quad (3b)$$

The result is plotted in Fig. 7 along with the functional forms $\mu = \mu_0 \exp(-z/\delta_\mu)$ and $G = G_0 \exp(-z/\delta_G)$ for which all the relevant parameters are obtained from the fit parameter to x , γ , and k . The first observation is that μ and G are not constant but increase exponentially with decreasing z . In other

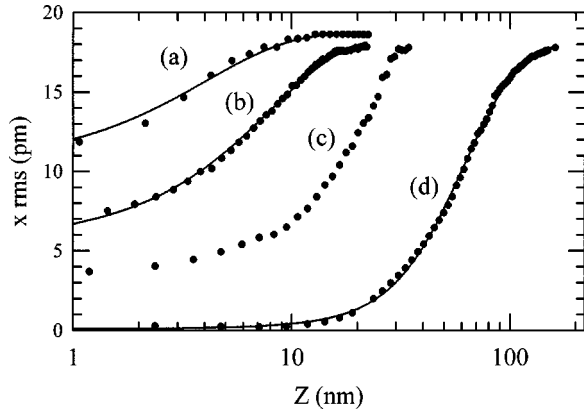


FIG. 6. The damping of the tip oscillation amplitude x as a function of the tip-sample distance is shown for different tip radii. All measurements were performed under vacuum condition with gold tips. In all measurements the nominal quality factor of the tuning-fork sensor was around 3000. Curves (a) and (b) are taken with the same tip and curve (c) a nominally larger tip. In case of curve (a), the tip was freshly prepared and the approach curve was the first one performed over the sample. The tip radius is not known with precision but is estimated from subsequent topographical imaging to be of the order of 10–20 nm. Curve (b) was taken after the tip approached several times and scanned the sample. Curve (d) was taken with a gold microsphere of 25 μm diameter attached to the end of the tuning fork, showing the strongest damping and the longest tip-sample interaction distance. The solid lines are obtained using a fit to Eq. (2). We obtained $\lambda = 5.5, 4.63,$ and 4.97 nm and $\delta = 3.35, 5.62,$ and 27.0 nm for curves (a), (b), and (d), respectively. No satisfactory fit was obtained for the data in curve (c).

words, the third body filling the tip-sample gap appears to become stiffer and more viscous as the tip approaches the substrate. Second, the magnitudes of G and μ are very different from those of regular condensed matter known in bulk

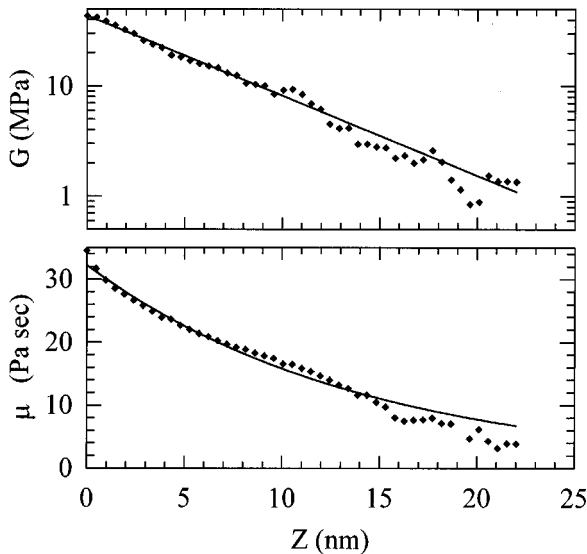


FIG. 7. The lower panel shows the viscosity of the third body filling the tip-sample gap as a function of the gap size (z). The top panel shows the corresponding shear modulus. The data points are obtained using the data set $\{x, \gamma\}$ and $\{x, k\}$ for μ and G , respectively, in Eqs. (3a) and (3b). We have assumed a contact area $A \approx (100 \text{ nm})^2$, which is poorly known. A is only estimated from topographical images and could be as small as $(30 \text{ nm})^2$. We have used $x_\infty = 18.6$ pm obtained from the fit in Fig. 2.

form. The viscosity here is about 4 orders of magnitude larger than that of most common liquids at 298 K, and the shear modulus is 1–2 orders of magnitudes smaller than that of common crystal materials.

V. ORIGIN OF THE SHEAR FORCES

So far we have assumed that the origin of the friction interaction is due to a material filling the tip-sample gap. However, in wear-free friction, dissipation can also originate from nonmechanical interactions such as Coulomb drag^{10,16,17} when conducting materials are involved. In some of these cases the role of phonons and electrons needs to be elucidated.¹⁶ Even quantum-mechanical effects are expected to contribute to friction. It is predicted that friction can be mediated through black-body fluctuation¹⁸ and even through vacuum fluctuation.¹⁹ The later contribution is understood in terms of the dynamic Casimir effect. Although the magnitude of such a quantum-mechanical friction force is expected to be very small, it is worth considering schemes that would allow us to measure its strength. We have evaluated viscous friction from all the above electromagnetic interactions as possible lossy interactions leading to the damping rate we measured in this work. We found that, although damping is expected in all cases, the estimated contributions are up to 10 orders of magnitude smaller than those measured in this experiment. We can also rule out Joule heating due to the oscillating charged image of the tip in the conducting sample. An overoptimistic upperbound estimation of such a Drude friction can be made by assuming that the colliding mass rate $M\gamma$ detected by the fork is given by the maximum possible collision mass rate given a scattering Drude electron gas, namely, $M\gamma = (\pi r^3 \xi) n_v m_e / \tau$, where n_v is the electron density, m_e the electron mass, and τ the mean electronic scattering time. The volume $\pi r^3 \xi$ includes all the electrons contributing to the formation of the charge image and can be approximated by that of an effective disk of thickness corresponding to the electrostatic screening length ξ and of a radius r of the tip. Taking the most optimistic values $n_v \approx 10^{22}/\text{cm}^3$, $\tau \approx 10^{-14}$ s, $\xi \approx 0.1$ nm as well as the worst case of a very large tip radius $r \approx 100$ nm, the largest detectable Drude collision mass rate should be $\gamma = 3 \times 10^{-6}/\text{s}$, which is 5 orders of magnitudes smaller than the noise level in Fig. 4. Consequently we can confidently rule out electromagnetic- as well as electrostatic-mediated interactions as being the origin of the viscous and elastic forces measured here. The same conclusion was previously reached by Ayars *et al.*²⁰ We are therefore led to speculate that the measured damping is mechanically mediated through adsorbate filling in the tip-sample gap. Although the measurements were conducted in a high-vacuum environment, we cannot exclude material buildup in the tip-sample gap. We do not know with certainty the nature of the material adsorbed in the tip-sample gap. It is likely to be water and hydrocarbon molecules. The exponential dependency of μ and G on the distance z hints that the adsorbate is located in a region where boundary conditions and surface potentials dominate over molecular interaction within the material filling the gap. Because the coefficient of viscosity is inversely proportional to the mobility of the molecules, one expects μ to be an exponential function of an activation energy. If we speculate that changing

the tip-sample distance increases linearly such an activation energy with decreasing z , this would definitely explain the exponential behavior seen in μ and γ . It is interesting to consider how the viscosity can be measured by a probe with oscillation amplitude less than an atomic size. The molecules in the third body are thermally agitated and experience a much larger motion. However, the average oscillation amplitude that is imposed by the tuning fork is there only to introduce a periodic velocity of the center of mass. The random motion of molecules statistically opposes such a displacement as described in a more general formalism by Persson in Ref. 10.

The stiffness to shear action can be explained by the adhesion energy of the adsorbate on both the tip and the sample surface. The adhesion forces are pulling the tip toward the sample. The oscillating tip experiences a tangential and a normal component to this force. The tangential component is the elastic force F_E given by Eq. 1(b). The normal component F_N is given by $F_E = -F_N \tan(\theta)$, where θ is the shear-strain angle in the xz plane. This angle is given by $\theta(z) \equiv [x - x(0)]/z$, where slippage of the third body is included through the term $x(0)$. For small tip amplitudes, such that $x - x(0) \ll z$ the two force components are related by $F_E = -F_N(x - x_0)/z$. We need now to establish a relation between F_N and γ_{AD} , the adhesion energy of the adsorbate. We can use the proximity-force theorem, which states that the force between plane and sphere of radius R is $F_N = 2\pi R e(z)$ where $e(z)$ is the potential energy per unit surface area which gives rise to the adhesion force between two parallel flat planes separated by z .²¹ We assume here that R is the radius of the tip. In the present case the maximum attraction between the tip and the sample is given using $e(0) \approx -2\gamma_{AD}$, assuming that the adhesion of the third body is the same on the sample and on the tip. Remembering that $F_E = kx$ we can establish that $e(z) = -kz[x/(x - x_0)]/(2\pi R)$ in order to get the adhesion energy γ_{AD} of the third body. The limit $e(0)$ can be evaluated making use of Eq. (2) in the limit of small z , which gives $\lim_{z \rightarrow 0} (x - x_0)/x_0 = z/\lambda$. We can therefore easily establish that $\gamma_{AD} \approx k_0 \lambda / (4\pi R)$, which in the case presented here is about $\gamma_{AD} \approx 1 \text{ J/m}^2$ (assuming a tip radius of 30 nm). The lower bound for the estimated adhesion energy would be 400 mJ/m^2 for an overestimated tip radius of 100 nm. Such an energy is much larger than pure van der Waals type of molecular interactions. It is comparable to adhesion energies of metal surfaces²² or to hydrogen bonding between the CO group and OH group.²³ It is interesting to note that since both γ_{AD} and λ are material constants independent of the tip geometry, the maximum spring constant k_0 of the tip-sample interaction has to scale with the tip radius. Since, on the other hand, k_0 scales like A , the contact area as determined from the condition $G_0 = \lambda(k_0/A)$ imposed on Eq. (2), we conclude that ideally A should also scale like the tip radius. Furthermore, since the maximum normal pressure in the tip-sample gap is given by $F_N/A = -2\pi R/A(2\gamma_{AD})$ we see that the pressure is independent of the tip geometry and is as expected only proportional to γ_{AD} .

The challenges we are facing now in tuning-fork shear-force microscopy are to control the nature of the adsorbate filling the tip-sample gap region as well as to control the size of the contact area at the tip level. Furthermore, since vis-

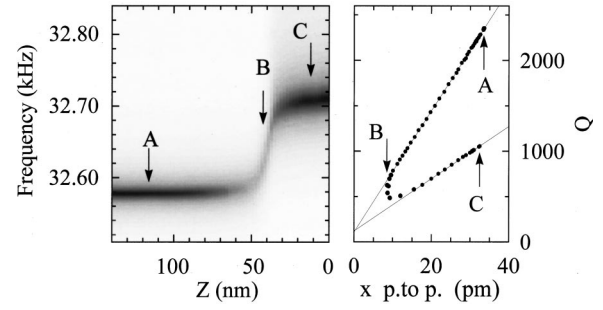


FIG. 8. Effect of a gold tip that is protruding too far outside the fork tine (i.e., probe length $230 \mu\text{m}$). The left panel is a gray-scale plot showing the mechanical resonance of the fork as the sample approaches the tip. The left panel shows the corresponding quality factor as a function of the tine oscillation amplitude. The breakdown of the viscously damped harmonic oscillator model is shown by the turning point in B for which the tip amplitude is reduced by mechanical bending of the probe. Details are discussed in the text. It is interesting to note that we measure two different exponential decay lengths, namely, $\delta_G = 6 \text{ nm}$, while that of the viscosity is $\delta_\mu = 14 \text{ nm}$.

cosity and adhesion are a thermally activated process, it will also be important to be able to repeat the measurements as a function of the temperature. It would also be very informative to reproduce such approach measurements in an ultrahigh-vacuum environment on clean tip and sample surfaces. Alternatively, similar measurements should also be reproduced with a thin-film liquid of controlled pH on the substrate.

VI. EFFECT OF THE TIP COMPLIANCE

It is important that the probe remains stiff in order to ensure maximum damping of the tuning fork. A question we addressed early in our investigations was to evaluate the tip bending due to the local shear forces. In the measurements presented above, the probe is a cut gold wire of $25 \mu\text{m}$ in diameter. Because of this particularly small diameter, it is necessary to make the free length l protruding outside the fork arm as short as possible. The condition to fulfill is that the probe elastic deformation amplitude should always be smaller than the tine amplitude. The probe elastic deformation is given by $x_P = F_E/k_P$, where k_P is the static spring constant of the protruding probe. Assuming a cylinder geometry for the probe, we estimate its spring constant using²⁴ $k_P = 3\pi E_{\text{gold}} r^4 / (4l^3)$ where r is the wire radius, and for gold, the Young modulus is $E_{\text{gold}} = 8 \times 10^{10} \text{ N/m}^2$. The value obtained for k_P is 10.9 kN/m . Since the largest elastic force measured in Fig. 5 was found to be of the order of $F_0 \approx 500 \text{ pN}$, the corresponding largest expected probe deformation of $x_P \approx F_0/k_P \approx 0.05 \text{ pm}$, which is much smaller than the measured x . We show in Fig. 8 an approach curve for which this condition is not fulfilled. A measurement showing a very similar behavior was reported a few years ago by Ruiter, Veerman, van der Werf, and van Hulst²⁵ and was not quite understood at the time. In the present case the probe length was $l = 230 \mu\text{m}$, which corresponds to $k_P \approx 350 \text{ N/m}$. Clearly this approach curve is different from the one measured in Fig. 3 with a shorter probe ($l = 75 \mu\text{m}$). An inspection of the dependence Q on the resonance amplitude x

shows that there are clearly two different regimes. In each of these regimes the resonator acts as a viscously damped harmonic oscillator. When the tip is approached from large z (indicated by A in Fig. 8), the Q of the resonance reduces as expected. At about 50 nm away from tip-sample contact (as defined by tunnel measurements) the Q reverses its trend and starts to increase with decreasing z . This turnaround behavior happens at the region indicated by B in Fig. 8. Q then increases linearly again until tunnel contact (point C). The different slopes (about half that of the region AB) indicates that not unexpectedly, the coupling to the driving force has increased by roughly a factor of 2. We infer from this measurement that at inflection point B the shear force is large enough that the probe starts to bend elastically. As a result the tip excursion is smaller and with it the friction at the sample is also smaller. The closer the tip is approached, the larger the restoring forces are and the more the probe bends at the expense of the oscillation amplitude at the tip. The contribution of the tip friction to the total losses reduces accordingly, leading to an increase of Q toward point C . The elastic forces measured by the tuning fork at point C corresponds to about 2.6 nN (peak), the corresponding elastic bending of the fork would be about $x_p \approx 10$ pm (peak), which matches the measured fork amplitude x in region B . This means that in region C the probe tip is clamped by the restoring shear-force interaction with the material filling the gap. From the analysis made above we are learning that the best indicator for normal operation in shear-force microscopy is the proportionality between Q and x . Departure from

this condition could be linked to an artifact due to tip bending.

VII. CONCLUSIONS

It is remarkable to see that in spite of its relatively large size, the tuning-fork sensor allows us to measure both friction and shear forces with a noise level as small as 1 pN. Measurements of such low friction-force levels are as far as we know unprecedented and are orders of magnitude better than standard friction-force scanning probe atomic force microscopes. One is presented here with a window of opportunity for the tuning-fork shear-force microscope, which offers the capability to measure viscous friction with the accuracy of a quartz-crystal microbalance but with the spatial resolution offered usually by friction-force microscopes. We have shown that the added advantage of the tuning-fork shear-force microscope is that it allows to measure friction for almost any arbitrary distance between the tip and the sample. Also we have shown how tuning-fork shear-force microscopy can be used for quantitative analysis in nanotribology provided that the contact area between sample and tip is controlled.

ACKNOWLEDGMENTS

We gratefully acknowledge lively discussions with Robert D. Grober and Lukas Novotny. This work was supported in part by the Bavarian ministry of education, research, and art under the new material (Neuwerkstoffe) research program.

-
- ¹M. O. Robbins and J. Krim, MRS Bull. **23**, 23 (1998).
²C. Mak and J. Krim, Phys. Rev. B **58**, 5157 (1998), and references therein.
³D. Y. C. Chan and R. G. Horn, J. Chem. Phys. **83**, 5211 (1985); B. Buschan, N. J. Israelachvili, and U. Landman, Nature (London) **374**, 607 (1995).
⁴A. R. Burns, J. E. Houston, R. W. Carpick, and T. A. Michalske, Phys. Rev. Lett. **82**, 1181 (1999).
⁵D. W. Carr, L. Sekaric, and H. G. Craigland, J. Vac. Sci. Technol. B **16**, 3821 (1998).
⁶H. Krömmmer, A. Erbe, A. Tilke, S. Manus, and R. H. Blick, Europhys. Lett. **50**, 101 (2000).
⁷B. H. Weigl and P. Yager, Science **283**, 346 (1999).
⁸P. J. A. Kenis, R. F. Ismagilov, and G. M. Whitesides, Science **285**, 83 (1999).
⁹E.g., R. P. Feynmann, *Lecture on Physics* (Addison-Wesley, Reading, MA, 1964), Vol. II.
¹⁰B. N. J. Persson, *Sliding Friction Physical Principles and Applications* (Springer, Berlin, 1998).
¹¹E. Betzig, P. L. Finn, and J. S. Weiner, Appl. Phys. Lett. **60**, 2484 (1992).
¹²R. Toledo-Crow, P. C. Yang, Y. Chen, and M. Vaez-Iravani, Appl. Phys. Lett. **60**, 2957 (1992).
¹³K. Karrai and R. D. Grober, Appl. Phys. Lett. **66**, 1842 (1995); Proc. SPIE **2535**, 69 (1995); Ultramicroscopy **61**, 197 (1995).
¹⁴R. D. Grober, J. Acimovic, J. Schuck, D. Hessman, P. Kindelmann, J. Hespanha, S. Morse, K. Karrai, I. Tieman, and S. Manus, Rev. Sci. Instrum. **71**, 2776 (2000).
¹⁵M. J. Gregor, P. G. Blome, J. Schöfer, and R. G. Ulbrich, Appl. Phys. Lett. **68**, 307 (1996).
¹⁶A. Dayo, W. Alnasrallah, and J. Krim, Phys. Rev. Lett. **80**, 1690 (1998).
¹⁷T. J. Gramila, J. P. Eisenstein, A. H. MacDonald, L. N. Pfeiffer, and K. W. West, Phys. Rev. B **47**, 12 957 (1993).
¹⁸B. N. J. Presson and A. I. Volokitin, Phys. Rev. Lett. **84**, 3504 (2000), and references therein.
¹⁹J. B. Pendry, J. Phys.: Condens. Matter **9**, 10 301 (1997).
²⁰E. Ayars, D. Aspnes, P. Moyer, and M. A. Paesler, J. Microsc. **196**, 591 (1999).
²¹J. Blocki, J. Randrup, W. J. Swiatecki, and C. F. Tsang, Ann. Phys. (N.Y.) **105**, 427 (1977).
²²J. N. Israelachvili, in *Intermolecular and Surface Forces* (Academic, London, 1991).
²³R. C. Thomas, J. E. Houston, R. M. Crooks, T. Kim, and T. A. Michalske, J. Am. Chem. Soc. **117**, 3830 (1995).
²⁴D. Sarid, *Scanning Force Microscopy* (Oxford University Press, New York, 1991).
²⁵A. G. T. Ruiter, J. A. Veerman, K. O. van der Werf, and N. F. van Hulst, Appl. Phys. Lett. **71**, 28 (1997).